OPEN ACCESS

ACTA METALLURGICA SLOVACA

2026, VOL. 32, NO. 3, 228-240

RESEARCH PAPER

Valorization of titanium production waste for selective Fe–Ti separation and concentrate production from titanomagnetite: response-surface optimization of chloride-assisted reduction roasting

Galymzhan Maldybayev[1,2], Argyn Korabayev[2], Rustam Sharipov[1,2], Ingkar Temirgali[1], Mehmet Deniz Turan[3], Omirserik Baigenzhenov[1,4]*

[1]*National Center on Complex Processing of Mineral Raw Materials of the Republic of Kazakhstan, 67. Jandossov Str., 050036, Almaty, Kazakhstan*
[2]*School of Materials Science and Green Technologies, Kazakh-British Technical University, 59. Tole bi Str., 050000, Almaty, Kazakhstan*
[3]*Department of Metallurgical and Materials Engineering, Fırat University, Elazığ 23119, Türkiye*
[4]*Department of Metallurgical Engineering, Satbayev University, 22a Satpaev Str., 050000, Almaty, Kazakhstan*

*Corresponding author: o.baigenzhenov@satbayev.university, tel.: +77074656502, Metallurgical engineering, / Satbayev university, 050013, Almaty

Received: 15.08.2026
Accepted: 23.08.2026

ABSTRACT

Titanium production wastes represent an underutilized secondary resource with potential value as functional additives in metallurgical processing. This study investigates the chloride-assisted reduction roasting of high-titanium titanomagnetite concentrate using semi-coke, spent titanium chlorinator melt (SMTC), a chloride-rich titanium production waste, and CaF2 to achieve selective Fe–Ti separation. A four-factor Box–Behnken response-surface design was applied to quantify the effects of roasting temperature and semi-coke, SMTC, and CaF_2 dosages on Fe grade, Fe recovery, TiO_2 grade, TiO_2 recovery, and iron metallization. RSM identified roasting temperature as the dominant process variable and delineated a broad high-performance region. The practically optimal conditions were 1200 °C, 20 wt.% semi-coke, 30 wt.% SMTC, and 4 wt.% CaF_2, yielding a magnetic fraction containing 91.24 wt.% Fe at 91.94% recovery and a non-magnetic fraction containing 62.78 wt.% TiO_2 at 96.04% recovery. Compared with NaCl, SMTC provided a substantially better balance between iron metallization and titanium partitioning. XRD and EPMA revealed extensive formation and coalescence of metallic α-Fe together with enrichment of rutile and magnesium titanate in the non-magnetic product. These findings demonstrate that chloride-rich titanium production waste can serve as an effective process additive for selective Fe–Ti separation, providing a dual pathway for titanomagnetite beneficiation and metallurgical waste valorization.

Keywords: Titanomagnetite; chloride-assisted roasting; spent chlorinator melt; Fe–Ti separation; magnetic separation

1. INTRODUCTION

Titanium is considered a strategically important metal due to its combination of high specific strength, low density, corrosion resistance, and heat resistance [1–3]. Due to these properties, titanium and its compounds are widely used in aerospace engineering, the chemical industry, energy, medicine, and metallurgy [4, 5]. The most widely produced titanium product is titanium dioxide, used primarily in pigment production, while titanium metal is in demand in high-tech industries [6]. Growing global demand for titanium products is accompanied by increased interest in developing new sources of titanium-containing raw materials. Along with traditional ilmenite and rutile ores, particular attention is being paid to complex titanomagnetite ores containing iron, titanium, vanadium, and a number of other valuable components [7–9]. Their integrated processing significantly improves the efficiency of mineral resource utilization and reduces waste generation.

Titanomagnetites are among the most promising types of complex raw materials, but their processing is complicated by the close interaction between iron and titanium minerals and by the formation of stable complex oxide phases. In traditional pyrometallurgical processes, titanium is predominantly concentrated in the slag phase, thereby limiting the feasibility of its comprehensive extraction and necessitating additional processing stages [10, 11]. Worldwide, various technologies have been developed for processing titanomagnetite ores, including reduction smelting, selective reduction followed by magnetic separation, hydrometallurgical treatment, and combined pyro-hydrometallurgical routes [12–14]. Pyrometallurgical processes generally achieve efficient iron recovery but often require high temperatures and produce titanium-rich slags that require further treatment. Hydrometallurgical routes may offer greater chemical selectivity but typically involve substantial reagent consumption and comparatively long processing times [15, 16]. In recent years, particular attention has been paid to reduction roasting technologies, which enable the selective reduction of iron-containing minerals at relatively low temperatures. This approach facilitates the subsequent efficient separation of the metallic and titanium phases using magnetic methods and reduces energy consumption compared to traditional smelting [17]. An increase in roasting efficiency is achieved by using various activating and chlorinating reagents, which intensify phase transformation processes and mass transfer [18]. Despite extensive research on the reduction roasting of titanomagnetite, the use of multicomponent chloride-bearing industrial residues as functional process additives remains underexplored. In particular, spent melts generated during titanium chlorination contain alkali, alkaline-earth, and iron chlorides that may alter reduction behaviour and Fe–Ti phase redistribution, yet their potential for promoting subsequent magnetic separation has received limited attention [19–21]. Moreover, direct comparisons between such complex chloride matrices and conventional single-component additives such as NaCl are scarce.

Accordingly, this study investigates the use of spent melt from titanium chlorinators (SMTC) as a chloride-bearing additive during reduction roasting of high-titanium titanomagnetite. The effects of roasting temperature, semi-coke dosage, SMTC dosage, and CaF_2 addition on iron metallization and Fe–Ti separation were systematically evaluated. NaCl was examined as a conventional reference additive, while XRD and EPMA were used to relate the metallurgical response to phase and microstructural transformations. The study therefore aims not only to improve selective Fe–Ti separation but also to establish a process route for the beneficial utilization of a chloride-bearing industrial by-product.

2. MATERIAL AND METHODS

2.1 Characteristics of the raw materials

Titanomagnetite concentrate with a particle size of 10-50 μm was chosen as the initial material for the research. The chemical composition of the main components of the titanomagnetite concentrate is shown in **Table 1**:

Table 1 Chemical composition of the high-titanium titanomagnetite concentrate used in this study

Component	TiO_2	Fe_{total}	V_2O_5	SiO_2	Al_2O_3	CaO	MgO
Content (wt.%)	18.7	51.0	0.13	4.5	4.5	2.8	5.7

Titanomagnetite and magnetite are the predominant iron-bearing phases in the concentrate. After beneficiation, the concentrate used in the present study is enriched in these phases, as reflected by the high Fe content (51.0 wt.%, Table 1). A small amount of ilmenite is also present. For the reduction of titanomagnetite concentrate, semi-coke with the characteristics presented in **Table 2** was selected.

The volatile matter of the semi-coke contains approximately 2.0–5.0 wt.% hydrogen, as summarized in **Table 3**. Spent melt of titanium chlorinators (SMTC) was used as a chlorinating additive.
Calcium fluoride (CaF_2, 98%; Sigmatec) was also used for low-temperature treatment.

Table 2 Characteristics of reducing agents

Reducing Agent	Content, %				
	Hydrogen	Volatile components	Ash content	Carbon	Sulfur
Semi-coke	2.0-5.0	3.0-8.0	3.5-6.0	88.0-93.0	0.3-0.5

Table 3 Chemical composition of the spent titanium chlorinator melt (SMTC)

Compounds	**Content, %**	**Compounds**	**Content, %**
$MgCl_2$	9.40	$AlCl_3$	0.76
KCl	20.0	$MnCl_2$	0.93
NaCl	15.0	SiO_2	0.80
$CaCl_2$	2.40	Cr	0.17
$FeCl_2$	19.50	TiO_2	1.10
$FeCl_3$	5.20	C	7.90
Moisture	12.84	Others	4.0

2.2 Reduction roasting and magnetic separation procedure
Reduction-roasting experiments were conducted using 50.0 g of high-titanium titanomagnetite concentrate (TMC) as the basis of the charge. Semi-coke was employed as the carbonaceous reducing agent, spent titanium chlorinator melt (SMTC) as the principal chloride-bearing process additive, and calcium fluoride (CaF_2) as an activating additive. In a separate comparative experimental series, NaCl was used as a conventional single-component chloride additive. Unless otherwise stated, the dosages of semi-coke, SMTC, NaCl, and CaF_2 are expressed as wt.% relative to the initial mass of TMC. The experimental programme was conducted sequentially to establish the effective operating ranges of the principal process variables before subsequent statistical optimization. The roasting temperature varied from 1000 to 1200 °C, the semi-coke dosage from 0 to 40 wt.%, the SMTC dosage from 0 to 40 wt.%, and the CaF_2 dosage from 0 to 5 wt.%. In each experimental series, the preferred condition identified at the preceding stage was retained while the next process parameter was varied. This preliminary sequential investigation was used to identify the technologically relevant operating region from which the factor ranges for subsequent response surface optimization were selected. For each roasting experiment, the prescribed amounts of TMC, semi-coke, SMTC and, where applicable, CaF_2 were thoroughly homogenized prior to charging into the crucible to ensure uniform distribution of the reducing and activating components throughout the reacting mixture. In the comparative NaCl series, NaCl was introduced in place of SMTC at the specified dosage and mixed with the remaining charge components using the same procedure. The prepared charge was transferred into a refractory crucible and subjected to reduction roasting in a BR-12N-6 electric resistance furnace. The furnace was heated at approximately 10 °C min^{-1} to the required roasting temperature, after which the charge was held isothermally for 60 min. After completion of the isothermal stage, the crucibles were cooled in the furnace to minimize rapid exposure of the reduced products to air and thereby limit secondary oxidation of metallic iron. The obtained roasted product (calcine) was removed from the crucible and crushed to break down thermally generated agglomerates. The calcine was subsequently ground to a particle size below 200 μm to promote liberation of the Fe-rich and Ti-bearing phases prior to magnetic separation. Magnetic separation of the ground calcine was performed using a 298-SE Davis-tube magnetic analyzer at a magnetic flux density of 0.20 T (≈159 kA m^{-1}). The selected magnetic-field intensity separated the strongly magnetic Fe-bearing particles from the predominantly non-magnetic Ti-bearing phases. Following magnetic separation, the magnetic and non-magnetic fractions were collected separately, dried to a constant mass, and weighed to determine their respective product yields. Representative samples of both fractions were subsequently subjected to chemical, mineralogical, and microstructural characterization.

The recovery of iron to the magnetic fraction and the recovery of TiO_2 to the non-magnetic fraction were calculated from the product yields and corresponding chemical compositions according to the conventional mass-balance relationship:

$$R_i = \frac{Y_j C_{i,j}}{C_{i,0}} \quad (1)$$

where R_i is the recovery of component i to the corresponding product (%), Y_j is the mass yield of product j expressed as a mass fraction, $C_{i,j}$ is the concentration of component i in product j, and $C_{i,0}$ is its concentration in the initial TMC.

Iron metallization was calculated as the proportion of metallic iron relative to total iron in the magnetic product:

$$M_{Fe} = \frac{Fe_{Me}}{Fe_{total}} \times 100 \quad (2)$$

The magnetic fraction was therefore evaluated primarily in terms of total Fe grade, metallic Fe content, degree of metallization, and Fe recovery, whereas the non-magnetic fraction was evaluated in terms of TiO_2 grade and TiO_2 recovery. These metallurgical indices were subsequently used to assess Fe–Ti separation efficiency and to define the response variables for statistical process optimization.

2.3 Statistical analysis and response surface methodology
Response surface methodology (RSM) was employed to statistically evaluate the combined effects of the principal roasting variables and to determine the operating conditions providing the most effective selective separation of iron and titanium. The ranges of the independent variables were selected on the basis of the preliminary sequential experiments described above, which identified the technologically relevant region for subsequent multivariable optimization [22, 23].
Four independent process variables were considered: roasting temperature (A), semi-coke dosage (B), spent titanium chlorinator melt (SMTC) dosage (C), and CaF_2 dosage (D). A four-factor Box–Behnken design (BBD) was adopted to evaluate the linear, interaction, and quadratic effects of these variables while limiting the number of experimental runs required for statistical optimization. The experimental factors were investigated at three coded levels (−1, 0, and +1). The actual and coded levels of the independent variables used in the Box–Behnken design are summarized in **Table 4**. The factor ranges were selected from the technologically relevant operating region identified by the preliminary sequential experiments, with particular emphasis on the conditions providing enhanced Fe–Ti separation

Table 4 Independent variables and coded levels used in the Box–Behnken design

Factor	**Variable**	**−1**	**0**	**+1**
A	Roasting temperature, °C	1100	1150	1200
B	Semi-coke dosage, wt.%	10	20	30
C	SMTC dosage, wt.%	20	30	40
D	CaF_2 dosage, wt.%	3	4	5

Because the objective of the process was selective Fe–Ti separation rather than maximization of a single metallurgical parameter, multiple responses were considered simultaneously. The principal responses were Fe content in the magnetic fraction (Y_1), Fe recovery to the magnetic fraction (Y_2), TiO_2 content in the non-magnetic fraction (Y_3), and TiO_2 recovery to the non-magnetic fraction (Y_4). The degree of iron metallization (Y_5) was additionally evaluated as a complementary response describing the extent of iron reduction.
The experimental responses were fitted to a second-order polynomial model:

$$Y = \beta_0 + \sum_{i=1}^{4} \beta_j X_j + \sum_{i=1}^{4} \beta_{jj} X_j^2 + \sum_{i<j}^{4} \beta_{jk} X_j X_k \quad (3)$$

where Yi denotes the predicted response (i=1–5); Xj and Xk are the coded independent variables corresponding to roasting temperature, semi-coke dosage, SMTC dosage, and CaF_2 dosage; β0 is the intercept; βj, βjj, and βjk are the linear, quadratic, and interaction coefficients, respectively.

The statistical significance and adequacy of the fitted models were evaluated by analysis of variance (ANOVA). Model significance was assessed using the F-value and associated *p*-value, with terms considered statistically significant at $p < 0.05$. Model quality was further evaluated using the coefficient of determination (R^2), adjusted R^2, predicted R^2, coefficient of variation (CV), adequate precision, and lack-of-fit test. Diagnostic plots of predicted versus experimental responses and internally studentized residuals were used to assess model agreement, residual distribution, and the presence of systematic deviations.

Three-dimensional response surface plots were generated to visualize the individual and combined effects of the process variables on Fe–Ti separation. Numerical multi-response optimization based on the desirability function was subsequently performed to identify the operating region that simultaneously maximized Fe grade and Fe recovery in the magnetic fraction and TiO_2 grade and TiO_2 recovery in the non-magnetic fraction, while maintaining a high degree of iron metallization. Model performance under the practically selected operating condition was evaluated using point predictions and by comparing predicted responses and confidence intervals with the corresponding experimental measurements. Statistical modelling and numerical optimization were performed using Design-Expert® software.

2.4 Analytical methods

The chemical compositions of the initial titanomagnetite concentrate and the products obtained after reduction roasting and magnetic separation were determined by inductively coupled plasma optical emission spectrometry (ICP-OES) using an Optima 2000 DV spectrometer (PerkinElmer, USA). X-ray fluorescence measurements were additionally performed using a Venus 200 wavelength-dispersive X-ray fluorescence spectrometer (PANalytical B.V., the Netherlands).

The phase compositions of the magnetic and non-magnetic fractions were characterized by X-ray diffraction (XRD) using a Rigaku SmartLab diffractometer (Rigaku Corp., Japan) with Co-Kα radiation (λ = 1.7890 Å), operated at 40 kV and 35 mA. Diffraction patterns were collected over a 2θ range of 10–90° with a step size of 0.02° and a scanning rate of 2° min^{-1}. Phase identification and semi-quantitative analysis were performed using PDXL 2 software (Rigaku) integrated with the ICDD PDF-2 database, followed by Rietveld refinement for quantitative phase evaluation.

Microstructural and local compositional characterization of the roasting products was performed by electron probe microanalysis (EPMA) using a JXA-8230 electron probe microanalyzer (JEOL, Japan). The magnetic and non-magnetic fractions were examined to evaluate the morphology and spatial association of Fe- and Ti-bearing phases and to support interpretation of phase redistribution during reduction roasting and subsequent magnetic separation. Complementary mineralogical observations were performed in reflected light using an OLYMPUS BX53 optical microscope equipped with a SIMAGIS XS-3CU digital camera and Mineral C7 image-analysis software. The chemical and mineralogical data obtained from these complementary analytical techniques were used, together with the metallurgical indices defined in Section 2.2, to evaluate iron reduction and Fe–Ti separation.

RESULTS AND DISCUSSION

3.1 Effect of roasting conditions on the selective separation of iron and titanium

The preliminary sequential experiments were conducted to establish the technologically relevant ranges of the principal roasting variables prior to multivariable optimization. Roasting temperature was examined first, followed sequentially by semi-coke, SMTC, and CaF_2 dosages, with the preferred condition identified at each stage retained in the subsequent experimental series. This approach enabled evaluation of the individual effects of the principal process variables on iron reduction and Fe–Ti partitioning while progressively defining the high-performance operating region for subsequent RSM analysis. According to the literature, the reduction of iron-containing phases to a metallic state in titanomagnetite systems begins at temperatures of approximately 940–993 °C [5, 24]. On the other hand, at temperatures above 1200 °C, sintering and agglomeration of the charge material are typically observed, which can impair phase liberation and reduce the effectiveness of subsequent magnetic separation [25]. Based on these considerations, a range of 1000–1200 °C was chosen in the present study to determine the optimal temperature regime for reduction roasting. For the preliminary temperature-screening series, the semi-coke dosage was fixed at 30 wt.% of the concentrate mass to maintain a sufficiently reducing environment across the investigated temperature interval. After the preferred roasting temperature had been identified, the semi-coke dosage was subsequently varied to determine the dosage providing the most favorable balance between iron reduction and Fe–Ti separation. The experimental conditions and results are presented in **Table 5**.

Table 5 Effect of roasting temperature on the selective separation of iron and titanium

Experiment number	Fraction	Yield, %	Content, %		Recovery, %	
			Fe_{total}/Fe_{Me}	TiO_2	Fe	TiO_2
1000 °C						
Exp. 1	Magnetic	40.81	67.33/43.0	19.86	53.88	43.35
	Non-magnetic	46.69	50.38	22.69	46.12	56.65
	LOI	12.50	-	-	-	-
	Total	100.00	51.00	18.70	100.0	100.0
1100 °C						
Exp. 2	Magnetic	47.49	69.02/50.0	15.76	64.27	40.03
	Non-magnetic	38.51	47.32	29.12	35.73	59.97
	LOI	14.00	-	-	-	-
	Total	100.00	51.00	18.70	100.0	100.0
1200 °C						
Exp. 3	Magnetic	52.98	70.60/55.0	8.99	73.35	25.46
	Non-magnetic	30.52	44.54	45.67	26.65	74.54
	LOI	16.50	-	-	-	-
	Total	100.00	51.00	18.70	100.0	100.0
Fixed conditions: TMC, 50 g; semi-coke, 15 g (30 wt.% relative to TMC); roasting time, 60 min. Variable: roasting temperature, 1000–1200 °C.						

From the results in **Table 5**, it follows that increasing the roasting temperature from 1000 to 1200 °C increases the yield and iron content in the magnetic fraction, with an iron recovery of 73.35% at 1200 °C. At the same time, a decrease in the yield of the non-magnetic fraction to 30.52% and an increase in the titanium dioxide content to 45.67% are observed, while the recovery of titanium dioxide reaches 74.54%. Thus, increasing the roasting temperature enhances the degree of iron metallization and improves phase differentiation, with optimum results achieved at 1200 °C, where favorable conditions for the phase separation of iron-bearing and titanium-bearing components are established. The beneficial effect of increasing the roasting temperature observed in the present study is consistent with previous investigations of titanomagnetite reduction followed by magnetic separation. Geng et al. [26] identified 1200 °C as the optimum reduction temperature for beach titanomagnetite concentrate, obtaining an iron product containing 90.28 wt.% Fe with 90.85% Fe recovery and a titanium concentrate containing 46.24 wt.% TiO_2 with 91.15% TiO_2 recovery. Similarly, reduction roasting of refractory titanomagnetite at 1200 °C followed by magnetic separation produced a magnetic concentrate containing 91.1 wt.% Fe at 92.9% recovery [27]. These findings support the present observation that temperatures near 1200 °C provide favorable conditions for the reduction of iron-bearing phases and subsequent Fe–Ti separation. However, the comparatively lower recoveries obtained at this stage of the present study (73.35% Fe and 74.54% TiO_2) indicate that temperature alone is insufficient to maximize separation efficiency, emphasizing the importance of optimizing reductant dosage and modifying additives in the subsequent experiments. During low-temperature reductive roasting, the magnetic properties of the products and the degree of separation of the iron-bearing and titanium-bearing phases are

controlled by several factors, among which the reducing agent is of primary importance. The reducing potential of the gas-solid environment generated within the system, determined by the composition and amount of the reducing agent, governs the equilibrium of iron oxide reduction reactions and, consequently, the direction and extent of the phase transformations. Varying the amount of reducing agent in the charge, or even eliminating it entirely, can lead to different conditions for the reduction reactions, potentially affecting the phase composition of the roasting products, their magnetic properties, and the efficiency of subsequent separation of iron and titanium. At the same time, such experiments allow us to assess the contribution of other charge components to the formation of the phase state of the low-temperature roasting products. Accordingly, the next stage of the research included an experimental study of the effects of reducing agent quantity and of its absence from the charge on the results of low-temperature reducing roasting of titanomagnetite concentrate. The experimental conditions and results used to determine the optimal reducing-agent dosage are presented in **Table 6** and **Fig. 1**.

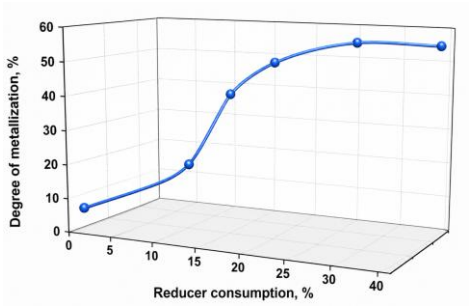

Fig. 1 Effect of reducing agent dosage on magnetic separation performance

Analysis of the results of experiments to determine the optimum dosage of the reducing agent shows that an increase in the dosage of the reducing agent has a decisive effect on both the depth of reduction of iron-containing phases and the nature of the phase and magnetic separation of the components of titanomagnetite concentrate. In the absence of a reducing agent (0 %), the process is predominantly thermally activated: iron recovery to the magnetic product is only 53.2%, while the proportion of metallic iron in the magnetic fraction remains extremely small (Fe_{Me} = 5.9 % at Fe_{total} = 55.86 %), which indicates a low degree of metallization and the predominance of oxide forms of iron. The addition of 10 wt.% semi-coke promoted iron reduction, increasing iron recovery in the magnetic fraction to 60.33%. The magnetic product contained 58.98 wt.% total Fe, of which 14.6 wt.% was present as metallic iron (FeMe), indicating the onset of significant metallization. Increasing the semi-coke dosage to 15 wt.% further promoted iron reduction and metallization: the FeMe content of the magnetic product increased to 38.7 wt.%, while Fetotal reached 62.05 wt.% and Fe recovery increased to 64.22%. At the same time, the selectivity of separation for titanium increases, since the content of titanium dioxide in the magnetic fraction is reduced to 10.35 %, and its main part is concentrated in the non-magnetic product (70.78 %). The most favorable combination of indicators is achieved with a reducing agent dosage of 20 %. Under these conditions, the recovery of iron into the magnetic product increases to 71.59 %, the content of total iron in the magnetic fraction reaches 70.21 %, and the share of metallic iron is 52.2 %, which indicates the formation of highly metallized roasted product (calcine). At the same time, the content of titanium dioxide in the magnetic fraction is minimal (7.79 %), and its recovery into the magnetic product is only 21.67 %, which indicates the maximum selectivity of magnetic separation and the most effective enrichment of the iron component. Although higher semi-coke dosages slightly increased the metallic-iron content, they did not improve overall separation performance and resulted in greater TiO_2 reporting to the magnetic fraction. Therefore, 20 wt.% semi-coke was selected as the preferred dosage based on overall Fe–Ti separation rather than maximum metallization alone. This behavior is consistent with previous studies showing that reductant dosage must be optimized with respect to overall Fe–Ti separation rather than metallization alone. Zhao et al. [27] reported that increasing the coal dosage during titanomagnetite reduction at 1200 °C progressively promoted the formation of metallic iron, whereas increasing the dosage from 25 to 30 wt.% produced no further phase transformation, indicating a diminishing benefit at excessive reductant addition.

Table 6 Effect of reducing agent dosage on magnetic separation performance

Experiment number	Fraction	Yield, %	Content, %		Recovery, %	
			Fe_{total}/Fe_{Me}	TiO_2	Fe	TiO_2
0%						
Exp. 1	Magnetic	48. 58	55. 86/5.9	20.07	53. 20	52.14
	Non-magnetic	43. 91	54.35	20.38	46. 80	47.86
	LOI	7. 51	-	-	-	-
	Total	100. 0	51.00	18.70	100. 0	100.0
10%						
Exp. 2	Magnetic	52. 17	58. 98/14.6	19. 64	60. 33	54.79
	Non-magnetic	37. 83	53. 48	22. 35	39. 67	45.21
	LOI	10. 00	-	-	-	-
	Total	100. 0	51.00	18. 70	100. 0	100. 0
15%						
Exp. 3	Magnetic	52. 78	62. 05/38.7	10. 35	64. 22	29.22
	Non-magnetic	36. 02	50.67	36. 75	35. 78	70.78
	LOI	11. 20	-	-	-	-
	Total	100. 0	51.00	18. 70	100. 0	100.0
20%						
Exp. 4	Magnetic	52. 00	70. 21/52.2	7. 79	71. 59	21.67
	Non-magnetic	32. 50	44. 58	45. 07	28. 41	78. 33
	LOI	15. 50	-	-	-	-
	Total	100. 0	51. 00	18. 70	100. 0	100. 0
30%						
Exp. 5	Magnetic	52. 98	70. 60/55.0	8.99	73. 35	25.46
	Non-magnetic	30. 52	44.54	45.67	26. 65	74. 54
	LOI	16. 50	-	-	-	-
	Total	100. 0	51.0	18. 70	100. 0	100.0
40%						
Exp. 6	Magnetic	52. 17	70. 88/55.4	10.34	72.51	28.86
	Non-magnetic	30. 05	46. 66	44.27	27.49	71.14
	LOI	17. 78	-	-	-	-
	Total	100. 0	51.0	18. 70	100. 0	100.0

Fixed conditions: TMC, 50 g; roasting temperature, 1200 °C; roasting time, 60 min. Variable: semi-coke dosage, 0–40 wt.% (0–20 g relative to TMC).

Similarly, Gao et al. [28] found that insufficient coal led to incomplete titanomagnetite reduction, whereas excessive coal, despite increasing the amount of metallic iron, promoted the formation of finer iron particles more closely associated with gangue phases, thereby adversely affecting subsequent separation. These observations agree well with the present results, in which 20 wt.% semi-coke provided the most favorable balance between iron metallization

and selective Fe–Ti partitioning. A further increase in the dosage of the reducing agent to 30 to 40 % does not lead to a significant improvement in separation performance, which is manifested in the stabilization of the content of iron and titanium dioxide in the products and minor changes in their recovery. These results indicate that further increases in semi-coke dosage yield only marginal improvements in iron reduction and provide no benefit to overall Fe–Ti separation performance. The results indicate that the amount of reducing agent significantly affects the degree of iron reduction and the magnetic characteristics of the roasting products. At the same time, even with an increased dosage of the reducing agent, the need to create conditions that ensure the selective separation of iron- and titanium-containing phases remains. In this regard, the further development of low-temperature reduction roasting is associated not only with regulating the reduction potential of the environment but also with controlling the chemical mechanism of interaction among the components of the charge. Of particular interest in this aspect is the influence of chlorine-containing additives, which can alter phase transformations, reduction kinetics, and the morphology of the resulting products.

Accordingly, the next stage of research was to study the influence of the nature and chlorine-containing additive, as well as the conditions of its absence, on the phase composition, magnetic properties of the roasting products and the efficiency of separation of the iron and titanium components. The conditions and results of experiments to determine the optimal consumption of chlorine-containing additives in the form of spent melts of titanium chlorinators (SMTC) are presented in **Table 7** and **Fig. 2**.

Table 7 Effect of SMTC dosage on magnetic separation performance

Experiment number	Fraction	Yield, %	Content, %		Recovery, %	
			Fe_{total}/Fe_{Me}	TiO_2	Fe	TiO_2
0 %						
Exp. 1	Magnetic	52.0	70.21/52.2	7.79	71.59	21.67
	Non-magnetic	32.50	44.58	45.07	28.41	78.33
	LOI	15.50	-	-	-	-
	Total	100.0	51.00	18.70	100.0	100.0
15%						
Exp. 2	Magnetic	50.08	77. 10/65.5	18.08	75.70	48.43
	Non-magnetic	31.32	39.56	30.79	24.30	51.57
	LOI	18.60	-	-	-	-
	Total	100.0	51.00	18.70	100.0	100.0
30%						
Exp. 3	Magnetic	49. 23	89. 45/77.0	9.79	86.35	25.78
	Non-magnetic	30.77	22.62	45.11	13.65	74.22
	LOI	20. 00	-	-	-	-
	Total	100.0	51.00	18.70	100.0	100.0
40%						
Exp. 4	Magnetic	47.75	92.14/78. 2	10.79	86.28	27.57
	Non-magnetic	30.25	23.14	44.8	13.72	72.43
	LOI	22.00	-	-	-	-
	Total	100.0	51.00	18.70	100.0	100.0

Fixed conditions: TMC, 50 g; semi-coke, 10 g (20 wt.% relative to TMC); roasting temperature, 1200 °C; roasting time, 60 min. Variable: SMTC dosage, 0–40 wt.% (0–20 g relative to TMC).

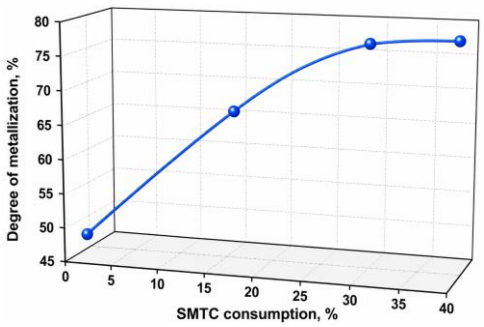

Fig. 2 Degree of metallization of the magnetic fraction as a function of SMTC dosage

Analysis of the experimental results presented in **Table 7** and **Fig. 2** shows that the addition of a chlorine-containing additive significantly affects the distribution of iron and titanium between the magnetic and non-magnetic fractions after low-temperature reduction roasting of titanomagnetite concentrate. In the absence of a chlorine-containing additive, the reduction roasting process leads to only a moderate redistribution of components. An increase in additive consumption up to 15% is accompanied by an improvement in separation performance. The strongest improvement was observed at SMTC dosages of 30–40 wt.%, where iron recovery remained approximately 86.3% while metallization increased from 77.0 to 78.2%. Over the same range, 72.43–74.22% of TiO_2 reported to the non-magnetic fraction. Simultaneously, the TiO_2 content in the magnetic product remained at 9.79–10.79%, indicating enhanced redistribution of iron- and titanium-bearing components between the magnetic and non-magnetic fractions. The experimental results demonstrate that the presence of SMTC substantially modifies the metallurgical response of the system, increasing iron metallization and promoting preferential partitioning of titanium into the non-magnetic fraction. These changes are consistent with intensified Fe–Ti phase redistribution during reduction roasting; the possible chloride-mediated pathways responsible for this behavior are discussed below on the basis of the SMTC–NaCl comparison and the subsequent phase and microstructural characterization. The pronounced effect of SMTC is consistent with the broader behavior of salt-assisted roasting systems reported for titanomagnetite-based materials. Chen et al. [29] demonstrated that molten-salt treatment can substantially modify the phase assemblage of Fe–Ti-bearing materials through the conversion of complex titanium-bearing phases into new salt-derived phases. Other studies of salt roasting of titanomagnetite have likewise shown that both salt dosage and roasting temperature strongly influence phase conversion and the subsequent distribution of Fe and Ti. The present results extend these observations to a reducing environment and, importantly, to a multicomponent chloride-bearing industrial residue, showing that SMTC can simultaneously promote iron metallization and Ti partitioning into the non-magnetic product. Accordingly, 30 wt.% SMTC was selected as the preferred dosage. Increasing the SMTC dosage to 40 wt.% produced only a marginal increase in metallization from 77.0 to 78.2%, while iron recovery slightly decreased from 86.35 to 86.28% and TiO_2 recovery in the non-magnetic fraction decreased from 74.22 to 72.43%. Thus, the additional SMTC consumption did not provide a meaningful improvement in overall Fe–Ti separation. To distinguish the effect of the multicomponent SMTC matrix from that of a conventional single-component chloride additive, NaCl was selected as a reference reagent. NaCl has been used in thermal treatment of Ti- and V-bearing materials and can modify phase transformations and salt-assisted mass transfer at elevated temperatures. A direct comparison with SMTC therefore provides a basis for assessing whether the observed improvement arises simply from chloride addition or from the more complex chemical composition of the spent chlorinator melt. In this regard, it is appropriate to conduct a comparative study of the influence of NaCl and SMTC on the processes occurring during the reduction roasting of titanomagnetite concentrate in order to identify differences in the mechanism of action of chlorine-containing additives, their effect on the phase composition of products and the efficiency of separation of components at a temperature of 1200 °C. The conditions and results of the experiments using NaCl as a chlorine-containing additive are presented in **Table 8** and **Fig. 3**.

Table 8 Effect of NaCl dosage on magnetic separation performance

Experiment number	Fraction	Yield, %	Content, %		Recovery, %	
			Fe_{total}/Fe_{Me}	TiO_2	Fe	TiO_2
0 %						
Exp. 1	Magnetic	52.00	70.21/52.2	7.79	71.59	21.67
	Non-magnetic	32.50	44.58	45.07	28.41	78.33
	LOI	15.50	-	-	-	-
	Total	100.0	51.00	18.70	100.0	100.0
10 %						
Exp. 2	Magnetic	44.80	77.07/58.6	22.30	67.70	53.43
	Non-magnetic	38.00	43.35	22.92	32.30	46.57
	LOI	16.20	-	-	-	-
	Total	100. 0	51.00	18.70	100.0	100.0
20 %						
Exp. 3	Magnetic	40.80	81. 20/66. 2	21.10	64.97	46.04
	Non-magnetic	42.10	42.44	23.97	35.03	53.96
	LOI	17.10	-	-	-	-
	Total	100.0	51.00	18.70	100.0	100.0
30 %						
Exp. 4	Magnetic	38.00	83.22/74.5	19.41	62.01	39.43
	Non-magnetic	44.80	43.25	25.28	37.99	60.57
	LOI	17.20	-	-	-	-
	Total	100.0	51.00	18.70	100.0	100.0
40 %						
Exp. 5	Magnetic	36.83	77.82/67.3	19.01	56.20	37.45
	Non-magnetic	46.27	48.28	25.28	43.80	62.55
	LOI	16.90	-	-	-	-
	Total	100.0	51.00	18.70	100.0	100.0

Charge composition: TMC (50 g); semi-coke (10 g); NaCl dosage: 0–40 wt.% (0–20 g, relative to the concentrate mass). Experimental conditions: Duration – 1 h, Temperature – 1200 °C.

Analysis of the experimental results showed that increasing the NaCl dosage during reduction roasting at 1200 °C had a limited effect on Fe–Ti partitioning between the magnetic and non-magnetic fractions. The yield of the magnetic fraction decreased from 44.80 to 36.83%, while its Fe content increased from 77.07 to 83.22 wt.%; however, Fe recovery decreased from 67.70 to 56.20%. TiO2 remained predominantly in the non-magnetic fraction, with its recovery increasing from 46.57 to 62.55%, indicating only partial redistribution of Ti-bearing phases without pronounced selective Fe–Ti separation. As the dosage of NaCl increases, a decrease in the yield of the magnetic fraction is observed (from 44.8 to 36.83 %) with a simultaneous increase in the iron content in the magnetic product (from 77.07 to 83.22 %), but the iron recovery decreases from 67.70 to 56.20 %. Titanium is predominantly concentrated in the non-magnetic fraction, with its recovery increasing from 46.57 to 62.55 %, indicating a partial redistribution of titanium-containing phases, but without any pronounced selective separation of iron.

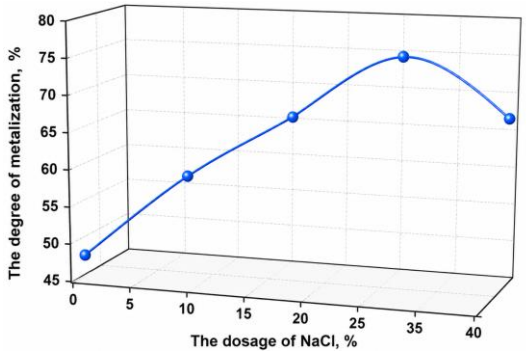

Fig. 3 The degree of metallization of the magnetic fraction as a function of sodium chloride

The comparatively limited performance of NaCl suggests that the addition of a single chloride salt was insufficient to reproduce the phase-separation behaviour observed with SMTC. Although NaCl increased the Fe content of the magnetic fraction at intermediate dosages, this was accompanied by a progressive decrease in iron recovery, indicating that enrichment of the magnetic product did not translate into improved overall Fe–Ti separation. These results suggest that the beneficial effect of SMTC cannot be attributed solely to the presence of NaCl or to chloride addition in general. Compared with NaCl, SMTC demonstrated markedly higher efficiency in promoting iron metallization and the selective enrichment of titanium in the non-magnetic fraction. At the selected SMTC dosage of 30 wt.%, metallization and iron recovery reached 77.0% and 86.35%, respectively. By comparison, at the same 30 wt.% dosage, NaCl yielded a metallization degree of 74.5% but an iron recovery of only 62.01%. Moreover, TiO_2 recovery in the non-magnetic fraction reached 74.22% with SMTC compared with 60.57% with NaCl. These results demonstrate that SMTC provides a substantially more favorable balance between iron metallization, iron recovery, and titanium partitioning than the conventional single-component chloride additive. The superior performance of SMTC relative to NaCl is consistent with a multicomponent chloride-assisted reaction pathway rather than with the action of a single chloride salt. SMTC contains $FeCl_2$, $FeCl_3$, $MgCl_2$, NaCl, KCl, and $CaCl_2$, several of which can participate in chloride-mediated transformations of Fe-bearing oxide phases at elevated temperatures. A plausible pathway involves transient conversion of iron from the Fe–Ti oxide lattice into chloride-bearing intermediates, particularly $FeCl_2$, followed by reduction to metallic Fe. The chloride-assisted decomposition of an ilmenite-type Fe–Ti oxide can be represented schematically by:

$$FeTiO_3 + Cl_2 + C \rightarrow FeCl_2 + TiO_2 + CO, \quad (4)$$

while $MgCl_2$, one of the major chloride components of SMTC, may provide an additional pathway:

$$FeTiO_3 + MgCl_2 \rightarrow FeCl_2 + MgO + TiO_2 \quad (5)$$

The transient $FeCl_2$ species can subsequently participate in reduction toward metallic iron, for example through:

$$FeCl_2 + H_2 \rightarrow Fe + 2HCl \quad (6)$$

The H_2 required for this pathway can be generated in situ rather than supplied externally. Hydrogen-containing volatile matter released from semi-coke can contribute to the reducing CO–H_2 atmosphere, while water vapor originating from residual moisture and chloride-associated hydrolysis/dehydration reactions can react with carbon through the water–gas reaction:

$$H_2O + C \rightarrow CO + H_2. \quad (7)$$

Thus, the combined presence of the carbonaceous reductant and chloride-rich SMTC can establish a locally reducing and chemically reactive environment favorable for the conversion of transient iron chloride species to metallic Fe. Within this proposed mechanism, temporary formation of chloride-bearing iron species can facilitate disruption of the original Fe–Ti–O association and promote selective transfer of iron toward the metallic phase, while titanium remains preferentially stabilized in oxide phases. The Mg-containing component of SMTC may additionally contribute to the stabilization of liberated titanium through the formation of Mg–Ti oxide phases. This interpretation is consistent

with the substantially superior metallurgical response obtained with SMTC compared with NaCl, and with subsequent XRD and EPMA observations showing the formation and coalescence of metallic Fe, together with enrichment of Ti in rutile- and magnesium-titanate-bearing non-magnetic domains. Because intermediate chloride species and gaseous reaction products were not directly characterized in the present experiments, the reactions above are proposed as chemically plausible pathways rather than as directly identified elementary reaction steps.

Because gaseous reaction products were not directly characterized, the specific contribution of volatile chloride species remains to be established. Previous studies have demonstrated that CaF_2 can promote iron reduction, metallic-iron particle growth, and subsequent Fe–Ti separation in titanomagnetite systems [27, 30]. Accordingly, the effect of CaF_2 dosage was examined to determine whether similar benefits could be achieved in the present SMTC-assisted system. The experimental conditions and results are presented in **Table 9** and **Fig. 4**.

Table 9 Effect of CaF2 dosage on magnetic separation performance

Experiment number	Fraction	Yield, %	Content, %		Recovery, %	
			Fe_{total}/Fe_{Me}	TiO_2	Fe	TiO_2
0 %						
Exp. 1	Magnetic	49.23	89.45/77.0	9.79	86.35	25.78
	Non-magnetic	30.77	22.62	45.11	13.65	74.22
	LOI	20.00	-	-	-	-
	Total	100.0	51.00	18.70	100.0	100.0
2 %						
Exp. 2	Magnetic	51.65	89.46/82.8	6.95	90.60	19.19
	Non-magnetic	28.75	16.67	52.56	9.40	80.81
	LOI	19.60	-	-	-	-
	Total	100.0	51.00	18.70	100.0	100.0
4 %						
Exp. 3	Magnetic	51.39	91.24/88.2	1.44	91.94	3.96
	Non-magnetic	28.61	14.37	62.78	8.06	96.04
	LOI	20.00	-	-	-	-
	Total	100.0	51.00	18.70	100.0	100.0
5 %						
Exp. 4	Magnetic	51.98	90.52/88.7	2.68	92.27	7.44
	Non-magnetic	27.82	14.18	62.22	7.73	92.56
	LOI	20.20	-	-	-	-
	Total	100.0	51.00	18.70	100.0	100.0

Fixed conditions: TMC, 50 g; semi-coke, 10 g (20 wt.% relative to TMC); SMTC, 15 g (30 wt.% relative to TMC); roasting temperature, 1200 °C; roasting time, 60 min. Variable: CaF_2 dosage, 0–5 wt.% (0–2.5 g relative to TMC).

Analysis of the data presented in **Table 9** shows that, in the absence of CaF2, even with a reducing agent and a chlorine-containing additive, the titanium content remains higher in the magnetic fraction, indicating incomplete redistribution and limited segregation efficiency of iron- and titanium-containing components. By adding CaF_2 in an amount of 4.0%, the most favorable combination of technological indicators is achieved: the iron content in the magnetic fraction increases to 91.24 %, with a degree of metallization of 88.2 % and recovery of 91.94 %, while the titanium dioxide content in the magnetic fraction decreases to 1.44 %. At the same time, the majority of the titanium-bearing phases is concentrated in the non-magnetic fraction, where the TiO_2 content reaches 62.78% and its recovery reaches 96.0%.

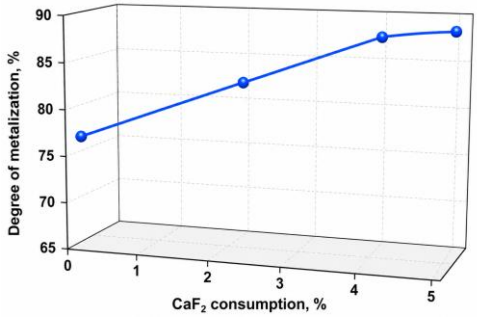

Fig. 4 The degree of metallization of the magnetic fraction depending on the dosage of CaF_2

These results indicate pronounced phase separation between the Fe-rich magnetic and Ti-rich non-magnetic components. Although increasing the CaF_2 dosage from 4 to 5 wt.% marginally increased iron recovery from 91.94 to 92.27% and metallization from 88.2 to 88.7%, TiO_2 recovery in the non-magnetic fraction decreased from 96.04 to 92.56%. Therefore, 4 wt.% CaF_2 was selected as the optimum dosage because it provided the best overall balance between iron recovery, titanium rejection from the magnetic fraction, and titanium recovery in the non-magnetic product. The optimum CaF_2 dosage identified in the present study is consistent with previous investigations of titanomagnetite reduction. Zhao et al. [27] likewise identified 4 wt.% CaF_2 as an effective dosage during reduction roasting of refractory titanomagnetite, reporting an increase in metallization from 85.5% without CaF_2 to 89.5% at 4 wt.% CaF_2, together with enhanced growth of metallic iron particles. Wu et al. [30] also demonstrated that CaF_2 can promote the individual enrichment of iron and titanium during reduction roasting followed by magnetic separation of titanomagnetite. The present results extend these observations by demonstrating a particularly pronounced improvement in Fe–Ti partitioning: at 4 wt.% CaF_2, the magnetic product contained 91.24 wt.% Fe with 91.94% Fe recovery, whereas 96.04% of TiO_2 was recovered in the non-magnetic fraction. Thus, the beneficial effect of CaF_2 in the present SMTC-assisted system is manifested not only in enhanced iron reduction but also in substantially improved selective partitioning of Fe and Ti between the two separation products.

The CaF_2 experiments demonstrate that a relatively small fluoride addition strongly influences the redistribution of Fe and Ti between the magnetic and non-magnetic products. Increasing the CaF_2 dosage from 0 to 4 wt.% increased iron recovery from 86.35 to 91.94% while decreasing the TiO_2 content of the magnetic fraction from 9.79 to 1.44%. Concurrently, TiO_2 recovery in the non-magnetic fraction increased from 74.22 to 96.04%. These changes indicate that CaF_2 promotes phase liberation and/or interfacial mass transfer during roasting, thereby facilitating the formation and separation of Fe-rich magnetic and Ti-rich non-magnetic products. The underlying effect may involve modification of the oxide–silicate reaction environment; however, transient fluoride-bearing phases were not directly identified in the present study, and the detailed mechanism therefore requires further investigation.

3.2 Response surface methodology and process optimization

To establish the operating window for selective Fe–Ti separation and to resolve the combined nonlinear effects of the principal roasting variables, a four-factor Box–Behnken response-surface design was applied. Roasting temperature (A), semi-coke dosage (B), SMTC dosage (C), and CaF_2 dosage (D) were varied systematically, while process performance was evaluated through five complementary metallurgical responses: Fe grade in the magnetic fraction (Y_1), Fe recovery to the magnetic fraction (Y_2), TiO_2 grade in the non-magnetic fraction (Y_3), TiO_2 recovery to the non-magnetic fraction (Y_4), and the degree of iron metallization (Y_5). The design comprised 29 experimental runs, including five centre-point replicates, thereby enabling simultaneous assessment of linear, interaction, and quadratic effects within the investigated factor space. The complete experimental matrix and measured responses are presented in **Table 10**.

Table 10 Box–Behnken experimental design and measured metallurgical responses

Run	T, °C	SC, wt. %	SMTC, wt. %	CaF_2, wt. %	Fe_{grade} wt. %	$Fe_{recovery}$ %	TiO_{2grade} wt.%	$TiO_{2recovery}$ %	Metallization %
1	1200	20.0	40.00	4.0	86.40	85.20	54.90	87.10	80.80
2	1200	10.0	30.00	4.0	82.50	78.40	48.20	76.80	72.50
3	1100	20.0	40.00	4.0	76.30	73.10	42.50	65.80	66.20
4	1200	30.0	30.00	4.0	88.60	87.90	57.40	89.20	83.80
5	1150	10.0	40.00	4.0	80.90	78.20	47.60	75.40	73.80
6	1150	10.0	20.00	4.0	75.80	71.90	40.50	63.20	65.90
7	1150	30.0	30.00	5.0	81.90	80.30	48.20	76.10	74.60
8	1100	10.0	30.00	4.0	71.40	66.80	36.50	55.40	58.20
9	1150	20.0	40.00	3.0	81.80	79.20	47.90	75.80	74.20
10	1150	30.0	30.00	3.0	80.20	77.90	46.50	73.20	72.80
11	1150	10.0	30.00	3.0	76.50	72.80	41.60	64.90	67.10
12	1150	10.0	30.00	5.0	78.20	74.90	43.10	68.20	69.50
13	1150	20.0	40.00	5.0	82.30	80.10	48.60	76.90	75.10
14	1200	20.0	20.00	4.0	88.50	87.20	56.80	89.40	82.40
15	1200	20.0	30.00	3.0	89.80	88.90	58.40	90.20	85.10
16	1150	20.0	30.00	4.0	86.15	85.10	54.80	87.20	81.00
17	1150	20.0	30.00	4.0	85.75	84.70	54.30	86.60	80.30
18	1150	20.0	30.00	4.0	86.30	85.30	55.10	87.40	81.10
19	1150	20.0	30.00	4.0	85.80	84.60	54.20	86.50	80.20
20	1100	20.0	30.00	5.0	73.50	69.80	38.90	60.20	61.40
21	1150	20.0	20.00	3.0	77.20	74.50	42.80	67.20	68.40
22	1200	20.0	30.00	5.0	90.52	92.27	62.22	92.56	88.70
23	1150	20.0	20.00	5.0	78.10	75.20	43.50	68.40	69.80
24	1100	30.0	30.00	4.0	74.80	71.20	40.10	61.50	64.10
25	1150	30.0	20.00	4.0	79.40	76.80	45.20	71.80	71.60
26	1150	30.0	40.00	4.0	84.70	83.50	53.10	84.50	78.80
27	1100	20.0	30.00	3.0	71.80	67.50	35.80	54.80	57.90
28	1100	20.0	20.00	4.0	72.10	68.30	38.20	58.60	60.50
29	1150	20.0	30.00	4.0	85.92	84.85	54.45	86.80	80.50

The experimental matrix covered a sufficiently broad response domain to resolve the transition from poorly reduced, weakly separated products to highly metallized and compositionally enriched fractions. Across the design space, Fe grade in the magnetic fraction varied from 71.40 to 90.52 wt.%, whereas Fe recovery increased from 66.80 to 92.27%. A similarly pronounced response was observed for titanium separation, with TiO_2 grade in the non-magnetic fraction ranging from 35.80 to 62.22 wt.% and TiO_2 recovery from 54.80 to 92.56%. The degree of iron metallization varied from 57.90 to 88.70%. In contrast to these large factor-induced variations, the five centre-point experiments exhibited only limited dispersion, indicating good experimental repeatability and providing a reliable estimate of pure experimental error. Collectively, these trends confirm that the selected factor ranges captured both strongly suboptimal and high-performance regimes and were therefore suitable for response-surface modelling and process optimization.

The statistical characteristics of the fitted models are summarized in **Table 11**.

Table 11. Statistical adequacy and predictive performance of the quadratic response-surface models.

Response	Model F-value	Model p-value	R^2	Adjusted R^2	Predicted R^2	CV, %	Adeq Precision	Lack-of-fit p
Fe grade	27.02	<0.0001	0.9643	0.9286	0.7954	1.88	17.706	0.0007
Fe recovery	19.27	<0.0001	0.9507	0.9014	0.7169	2.80	14.881	0.0004
TiO_2 grade	16.34	<0.0001	0.9423	0.8847	0.6694	5.18	13.409	0.0006
TiO_2 recovery	27.51	<0.0001	0.9649	0.9298	0.7986	4.13	16.734	0.0003
Metallization	17.56	<0.0001	0.9461	0.8922	0.6911	3.77	14.044	0.0006

All five quadratic models were highly significant ($p < 0.0001$), confirming that the selected process variables collectively accounted for a substantial proportion of the experimentally observed variation. The coefficients of determination were consistently high, ranging from $R^2 = 0.9423$ for TiO_2 grade to $R^2 = 0.9649$ for TiO_2 recovery, while the adjusted R^2 values remained between 0.8847 and 0.9298. Particularly strong predictive performance was obtained for Fe grade and TiO_2 recovery, with predicted R^2 values of 0.7954 and 0.7986, respectively. Fe recovery also retained useful predictive capability (predicted $R^2 = 0.7169$), whereas the somewhat larger differences between adjusted and predicted R^2 for TiO_2 grade and metallization indicate that predictions for these responses should be interpreted more conservatively outside the immediate vicinity of the experimental observations. The adequacy of the models was further supported by signal-to-noise ratios substantially above the accepted threshold: Adeq Precision ranged from 13.409 to 17.706, demonstrating that all five models provided sufficient discrimination across the investigated design space. The coefficients of variation were low (1.88–5.18%), consistent with satisfactory experimental precision relative to the magnitude of the measured responses. Nevertheless, the lack-of-fit tests were statistically significant for all five responses ($p = 0.0003$–0.0007), indicating that the quadratic polynomials do not capture all local features of the experimental response surfaces. This statistical significance is partly associated with the very small pure-error variance provided by the closely clustered centre-point replicates, which makes the lack-of-fit test sensitive to relatively small systematic deviations between the fitted surfaces and individual experimental observations. At the same time, the consistent significance of the quadratic terms for all five responses confirms pronounced response curvature, making lower-order linear or two-factor-interaction models unsuitable for describing the observed behaviour. A full cubic model was not adopted because the present 29-run four-factor Box–Behnken design does not provide sufficient independent information for reliable estimation of all cubic terms and would require additional experimental runs. The significant lack-of-fit therefore limits the models primarily with respect to precise point-by-point prediction rather than their use for identifying the direction and relative magnitude of factor effects, response curvature, and the location of the high-performance operating region.

Accordingly, the fitted models were interpreted together with the predicted-versus-actual plots, residual diagnostics, predicted R^2 values, and experimental validation, and were used as empirical optimization tools within the investigated factor space rather than as universally predictive mechanistic models.

Analysis of variance revealed a consistent hierarchy in the influence of the four process variables across the five metallurgical responses. Roasting temperature (A) exerted by far the strongest linear effect, followed by semi-coke dosage (B) and SMTC dosage (C), whereas the linear contribution of CaF_2 (D) was comparatively weak and statistically insignificant within the investigated range. This ordering was reproduced for Fe grade, Fe recovery, TiO_2 grade, TiO_2 recovery, and iron metallization, indicating that the major responses were governed by a common underlying progression of reduction and Fe–Ti phase separation rather than by unrelated response-specific effects. The strong and systematic influence of temperature is particularly important because simultaneous improvements in Fe enrichment, Fe recovery, TiO2 upgrading, and metallization indicate that increasing thermal severity promotes the overall transformation required for subsequent magnetic separation, rather than improving only a single performance indicator.

The dominant effect of temperature can be rationalized by the strongly temperature-dependent progression of iron-oxide reduction and the associated restructuring of Fe–Ti-bearing phases during roasting [27]. Increasing the temperature promotes the progressive reduction of Fe-bearing oxide phases and the formation and growth of metallic iron, thereby facilitating its subsequent recovery by magnetic separation. The present RSM analysis quantitatively confirms this behaviour within the investigated multicomponent system, identifying temperature as the principal factor governing not only iron metallization but also Fe enrichment and titanium redistribution into the non-magnetic product. Semi-coke provides the reducing capacity required for these transformations, explaining its positive but secondary contribution relative to temperature; thus, increasing carbon dosage cannot fully compensate for insufficient thermal activation. SMTC also exerted a statistically significant positive linear effect, consistent with its role in promoting phase transformation and redistribution during roasting rather than merely increasing the reducing potential of the charge.

The second-order terms provide additional insight into the existence of a finite operating optimum. The quadratic contributions A^2, B^2, C^2, and D^2 were statistically significant for all five responses, and their negative coefficients indicate downward curvature of the fitted response surfaces within the experimental domain. Consequently, improvements achieved by increasing temperature or reagent dosage progressively diminish as the upper region of the design space is approached. This effect is particularly relevant for semi-coke and SMTC: once sufficient reducing capacity and chloride-assisted transformation have been established, further reagent addition provides only marginal metallurgical benefit. The behaviour of CaF_2 is also noteworthy. Although its linear term was not significant over 3–5 wt.%, the significance of D^2 indicates that its effect cannot be regarded as negligible; rather, CaF_2 acts predominantly through a nonlinear response, with the process favouring an intermediate dosage instead of either boundary of the investigated range. These curvature effects provide the statistical basis for subsequent multi-response optimization and, importantly, argue against simply maximizing the consumption of individual reagents. Pairwise interactions were generally much weaker than the corresponding main and quadratic effects. Most two-factor interaction terms were not statistically significant, indicating that the principal variation in process performance is explained by the individual effects of temperature and reagent dosage, together with their response curvature. This does not imply complete independence of the process variables; rather, within the investigated factor ranges, strong synergistic or antagonistic pairwise interactions were not the primary source of response variation. A limited interaction between temperature and SMTC was evident for the Fe grade, suggesting that the contribution of the chloride-bearing additive becomes more pronounced as thermal activation approaches sufficiency. Overall, however, the response structure was dominated by temperature and by nonlinear dosage effects, which is consistent with the broad curved maxima subsequently observed in the response-surface plots.

The fitted second-order models, formulated as described in Section 2.3, were subsequently evaluated using predicted-versus-actual agreement and residual diagnostics before being applied to response-surface interpretation and multi-response optimization.

As shown in **Fig. 5**, the predicted-versus-actual plots exhibit close correspondence between the calculated and experimental responses for both Fe grade and TiO_2 recovery, with the data distributed predominantly along the ideal agreement line.

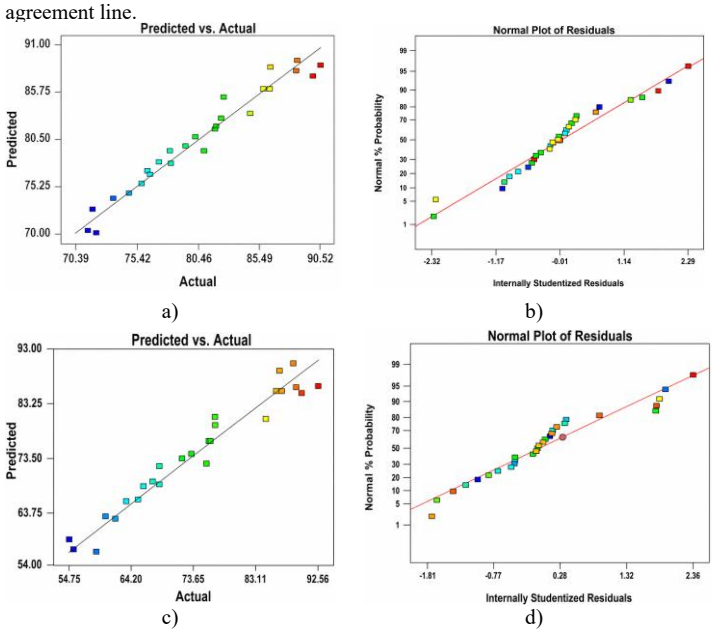

Fig. 5 Model diagnostic plots for the quadratic RSM models: (a) predicted versus actual Fe grade; (b) normal probability plot of residuals for Fe grade; (c) predicted versus actual TiO_2 recovery; and (d) normal probability plot of residuals for TiO_2 recovery.

The corresponding normal probability plots show an approximately linear distribution of the internally studentized residuals, without pronounced departures indicative of extreme outliers. In addition, the studentized residuals remained within the conventional ±3 limits. Taken together, these diagnostics support the internal consistency of the fitted models and indicate that, despite the statistically significant lack-of-fit, the quadratic equations remain suitable for describing the principal response trends and locating the high-performance region within the investigated experimental domain, while precise point-wise predictions should be interpreted with appropriate caution.

The three-dimensional response surfaces in **Fig. 6** provide a graphical representation of the factor effects identified by ANOVA.

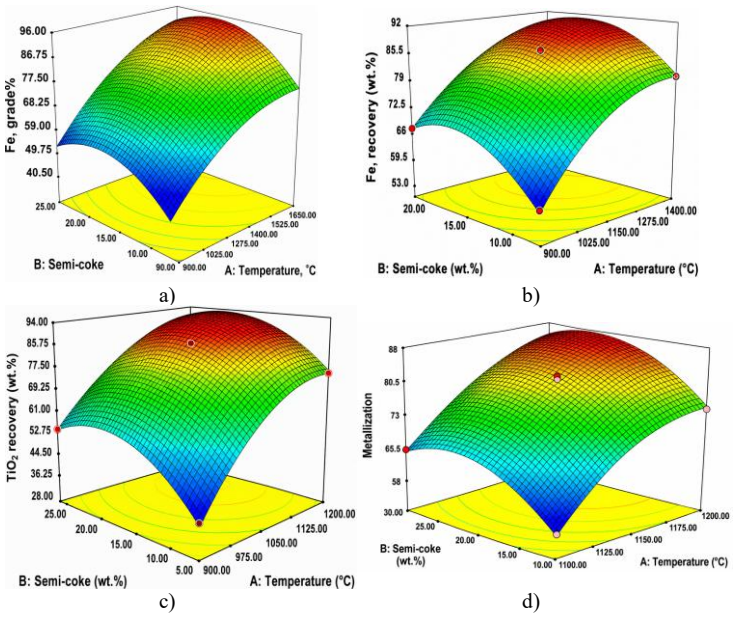

Fig. 6 Three-dimensional response-surface plots showing the effects of roasting temperature and semi-coke dosage on (a) Fe grade, (b) Fe recovery, (c) TiO_2

recovery, and (d) iron metallization at SMTC = 30.91 wt.% and CaF_2 = 4.16 wt.%.

For all four illustrated responses, increasing the roasting temperature toward 1200 °C produced a pronounced improvement in process performance, confirming temperature as the dominant operating variable. Fe grade and Fe recovery increased concurrently, indicating that enhanced reduction was accompanied not merely by Fe enrichment but also by more effective transfer of iron to the magnetic product. TiO_2 recovery in the non-magnetic fraction increased in parallel with iron metallization, demonstrating that the progression of iron reduction was coupled with increasingly effective Fe–Ti partitioning between the two separation products. The effect of semi-coke was distinctly nonlinear: increasing its dosage from the lower end of the investigated range improved all responses, whereas the incremental gain diminished at higher dosages. The resulting surface curvature is consistent with the significant negative B^2 coefficients and indicates a broad high-performance region rather than a continuously increasing benefit from additional reductant.

The overall desirability surface shown in **Fig. 7** identifies a broad high-performance region at elevated roasting temperature and intermediate semi-coke dosage. Numerical multi-response optimization located the maximum desirability (D=0.985) at 1200 °C, 24.06 wt.% semi-coke, 30.91 wt.% SMTC, and 4.16 wt.% CaF_2. At these conditions, the models predicted an Fe grade of 91.07 wt.%, Fe recovery of 91.55%, TiO_2 grade of 61.67 wt.%, TiO_2 recovery of 95.90%, and iron metallization of 87.67%. The corresponding 95% confidence intervals were 89.71–92.44% for Fe grade, 89.04–94.06% for Fe recovery, 58.84–64.49% for TiO_2 grade, 92.36–99.43% for TiO_2 recovery, and 84.53–90.82% for metallization.

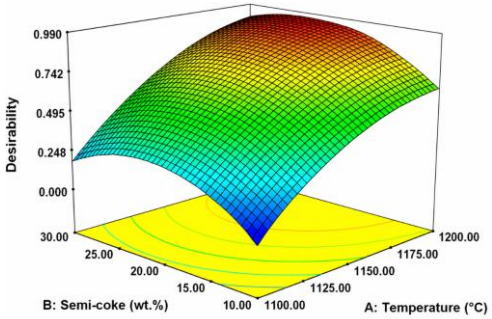

Fig. 7 Overall desirability response surface for simultaneous optimization of Fe–Ti separation as a function of roasting temperature and semi-coke dosage at SMTC = 30.91 wt.% and CaF_2 = 4.16 wt.%

Although the purely numerical optimum required approximately 24 wt.% semi-coke, the experimentally selected condition of 1200 °C, 20 wt.% semi-coke, 30 wt.% SMTC, and 4 wt.% CaF_2 was located within the high-performance region predicted by the models. At this practically selected operating point, the experimental Fe grade, Fe recovery, TiO_2 grade, TiO_2 recovery, and metallization were 91.24 wt.%, 91.94%, 62.78 wt.%, 96.04%, and approximately 88.2%, respectively. Point prediction at the same operating conditions yielded 90.85 wt.% Fe, 90.55% Fe recovery, 60.75 wt.% TiO_2, 94.93% TiO_2 recovery, and 86.63% metallization. All experimentally measured responses fell within the corresponding 95% confidence intervals of the RSM predictions. The close agreement indicates that, despite the statistically significant lack of fit, the response-surface models provide a reasonable local representation of the experimentally selected operating condition. Considering the marginal predicted gain associated with increasing the semi-coke dosage from 20 to approximately 24 wt.% and the additional reductant consumption involved, the condition of 1200 °C, 20 wt.% semi-coke, 30 wt.% SMTC, and 4 wt.% CaF_2 was therefore retained as the practically rational operating point for Fe–Ti separation.

3.3 Structural characterization of roasted products

The magnetic and non-magnetic products obtained under the practically selected operating conditions (1200 °C, 20 wt.% semi-coke, 30 wt.% SMTC, and 4 wt.% CaF_2) were selected for detailed phase and microstructural characterization. Under these conditions, the magnetic product contained 91.24 wt.% Fe with an iron recovery of 91.94%, whereas the non-magnetic product contained 62.78 wt.% TiO_2 with a TiO_2 recovery of 96.04%. XRD analysis, **Fig. 8**, **Table 12**, was subsequently employed to identify the crystalline phases responsible for this separation behavior, while EPMA was used to examine the corresponding microstructural and elemental partitioning between the magnetic and non-magnetic products.

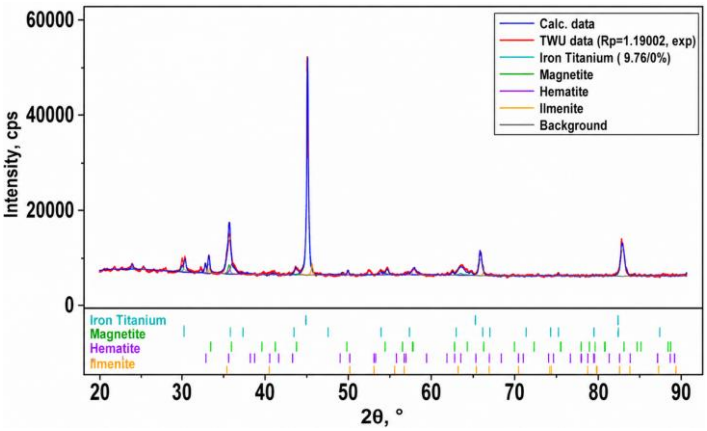

Fig. 8 XRD pattern of the magnetic fraction

Table 12 Results of diffractometric analysis of the magnetic fraction

Component	Formula	Mass fraction, %
α-Fe (Ti solid solution)	$(Fe_{39}Ti)_{0.05}$	46.6
Magnetite	Fe_3O_4	35.5
Hematite	Fe_2O_3	8.3
Ilmenite	$FeTiO_3$	9.6

The magnetic fraction contained Ti-bearing α-Fe as the largest individual crystalline phase, accounting for 46.6 wt.%. The intense diffraction maximum at $2\theta \approx 44.7°$ is consistent with the (110) reflection of α-Fe and confirms substantial formation of metallic iron during reduction roasting. In addition to metallic iron, residual oxide phases were identified in the magnetic fraction: magnetite (35.5 wt. %), ilmenite (9.6 wt. %) and hematite (8.3 wt. %). The presence of magnetite and hematite indicates incomplete reduction of some iron-containing minerals, while the preservation of a small amount of ilmenite indicates the transition of some titanium-containing phases into a magnetic product due to incomplete liberation of mineral intergrowths or insufficient selectivity of the reduction process. The coexistence of metallic α-Fe with residual iron oxides indicates extensive but incomplete reduction. Nevertheless, formation of a discrete metallic iron phase provides the magnetic contrast required for subsequent separation from the predominantly non-magnetic Ti-bearing phases. The observed phase assemblage is consistent with previous studies of titanomagnetite reduction roasting followed by magnetic separation. Zhao et al. [27] reported that progressive reduction of titanomagnetite at 1200 °C resulted in the formation of metallic Fe accompanied by residual Ti-bearing phases, with the relative intensity of metallic-iron reflections increasing as reduction proceeded. Their results further demonstrated that the development and growth of discrete metallic Fe particles are critical for their subsequent liberation and recovery by magnetic separation. The present XRD results exhibit the same general phase-separation tendency, although the persistence of magnetite, hematite, and ilmenite indicates that reduction was not complete under the investigated conditions.

The phase assemblage of the non-magnetic product differed markedly from that of the magnetic fraction. As shown by the XRD pattern in **Fig. 9** and the corresponding phase analysis in **Table 13**, the non-magnetic fraction was dominated by silicate and Ti-bearing oxide phases, with no metallic Fe identified among the principal crystalline constituents.

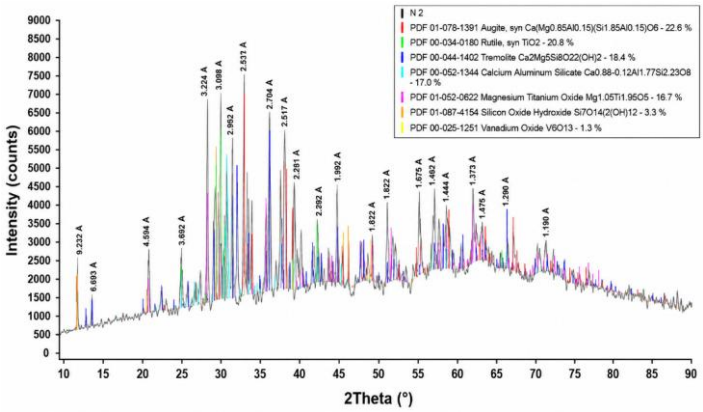

Fig. 9 XRD pattern of the non-magnetic fraction

The results of the diffractometric analysis of the non-magnetic fraction are presented in Table 13.

Table 13 Results of X-ray diffraction (XRD) of the non-magnetic fraction

Compound Name	Formula	S-Q
Augite, syn	$Ca(Mg_{0.85}Al_{0.15})(Si_{1.85}Al_{0.15})O_6$	22.6%
Rutile, syn	TiO_2	20.8%
Tremolite	$Ca_2Mg_5Si_8O_{22}(OH)_2$	18.4%
Calcium Aluminum Silicate	$Ca_{0.88}Al_{1.77}Si_{2.23}O_8$	17.0%
Magnesium Titanium Oxide	$Mg_{1.05}Ti_{1.95}O_5$	16.7%
Hydrated silicon oxide	$Si_{74}O_{142}(OH)_{12}$	3.3%
Vanadium Oxide	V_6O_{13}	1.3%

The non-magnetic fraction is characterized by a complex mineral composition, represented mainly by silicate and titanium-containing phases. The main minerals are augite (22.6 wt. %), rutile (20.8 wt. %), tremolite (18.4 wt. %), calcium aluminosilicate (17.0 wt. %) and magnesium titanate $Mg_{1.05}Ti_{1.95}O_5$ (16.7 wt.%). Minor amounts are represented by silicon hydroxide (3.3 wt. %) and vanadium oxide (1.3 wt. %). The high content of rutile and magnesium titanate indicates that, during the reduction roasting process, titanium is predominantly concentrated in stable oxide phases that are nonmagnetic. The occurrence of a substantial magnesium-titanate fraction is also consistent with the proposed participation of Mg-bearing components of SMTC in the phase-redistribution process. In the proposed pathway, Mg-bearing species generated from the chloride-rich additive may interact with TiO_2 released during decomposition of Fe–Ti-bearing phases, thereby contributing to the stabilization of titanium within non-magnetic Mg–Ti oxide phases. This interpretation provides a possible link between the multicomponent composition of SMTC and the experimentally observed enrichment of titanium in the non-magnetic product. Importantly, the bulk TiO_2 grade of the non-magnetic product should not be interpreted as the rutile content alone, because XRD demonstrates that titanium is partitioned among multiple Ti-bearing phases, particularly rutile and magnesium titanate. The formation of the magnesium titanate phase ($Mg_{1.05}Ti_{1.95}O_5$) is attributed to the interaction of TiO_2 with magnesium-containing components of the original titanomagnetite at elevated temperatures, while the formation of rutile is associated with the redistribution of titanium after the reduction of iron-containing phases. The predominance of silicate minerals (augite, tremolite and calcium aluminosilicate) is explained by the transition of rock-forming components into a non-magnetic product after preferential recovery of metallic iron into the magnetic fraction. The predominance of silicate and Ti-bearing oxide phases, together with the comparatively low abundance of Fe-bearing magnetic phases, is consistent with preferential transfer of metallic iron to the magnetic product and enrichment of titanium in the non-magnetic fraction. A comparable Fe–Ti phase-partitioning behavior was reported by Wang et al. [31] during coal-based direct reduction of vanadium–titanium magnetite. Their XRD analysis showed that reduction promoted the conversion of Fe-bearing phases to metallic Fe, while Ti remained associated predominantly with oxide phases, including a stable $(Mg,Fe)Ti_2O_5$ phase. Subsequent grinding and magnetic separation preferentially recovered metallic iron into the magnetic concentrate, whereas most of the titanium reported to the non-magnetic product. Under their optimized conditions, an Fe concentrate containing 76.78 wt.% Fe was obtained with 93.41% Fe recovery, while Ti recovery in the non-magnetic product reached 87.07%. These findings are consistent with the phase-partitioning tendency observed in the present study, although the SMTC/CaF_2-assisted roasting route achieved a substantially higher TiO_2 recovery in the non-magnetic fraction (96.04%) and a higher Fe grade in the magnetic product (91.24 wt.%). The comparison therefore supports the interpretation that selective reduction of Fe-bearing phases, combined with retention and redistribution of titanium within non-magnetic oxide phases, is fundamental to effective Fe–Ti separation.

The EPMA observations of the magnetic fraction (**Fig. 10**) provide microstructural support for the phase transformations identified by XRD.

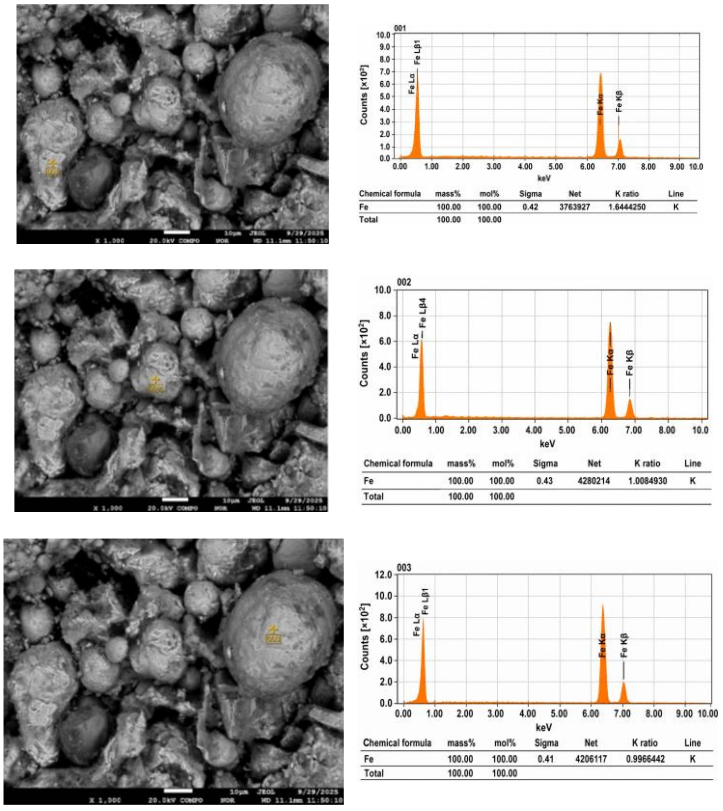

Fig. 10 EPMA image and point-analysis spectra of the magnetic fraction obtained after reduction roasting under the selected operating conditions (×1000).

Coarse Fe-rich particles with predominantly rounded to spheroidal morphologies are clearly distinguished from the surrounding non-metallic matrix, indicating substantial reduction followed by coalescence and local sintering of metallic iron. Point analyses of these domains confirm their Fe-rich character, consistent with the α-Fe phase identified by XRD. Importantly, the development of discrete and

coarsened Fe-rich particles increases the magnetic and physical contrast between the reduced iron phase and the surrounding Ti-bearing oxide–silicate matrix, thereby providing a microstructural basis for the high Fe grade and recovery achieved during subsequent magnetic separation.

Complementary EPMA examination of the non-magnetic fraction at two magnifications (**Figs. 11** and **12**) was used to assess both the overall morphology of the Ti-bearing product and the local elemental partitioning within individual oxide–silicate domains.

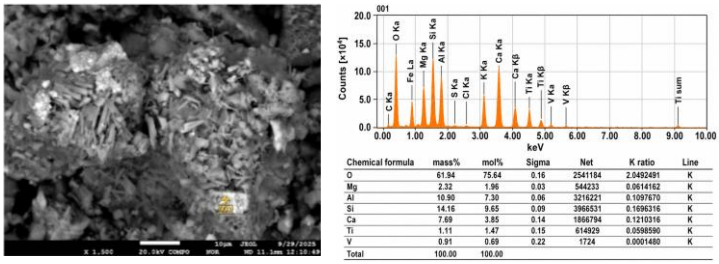

Chemical formula	mass%	mol%	Sigma	Net	K ratio	Line
O	61.94	75.64	0.16	2541184	2.0492491	K
Mg	2.32	1.96	0.03	544233	0.0614162	K
Al	10.90	7.30	0.06	3216221	0.1097670	K
Si	14.16	9.65	0.09	3966531	0.1696316	K
Ca	7.69	3.85	0.14	1866794	0.1210316	K
Ti	1.11	1.47	0.15	614929	0.0598590	K
V	0.91	0.69	0.22	1724	0.0001480	K
Total	100.00	100.00				

Fig. 11 EPMA image and point-analysis spectra of the non-magnetic fraction obtained after reduction roasting under the selected operating conditions (×1500).

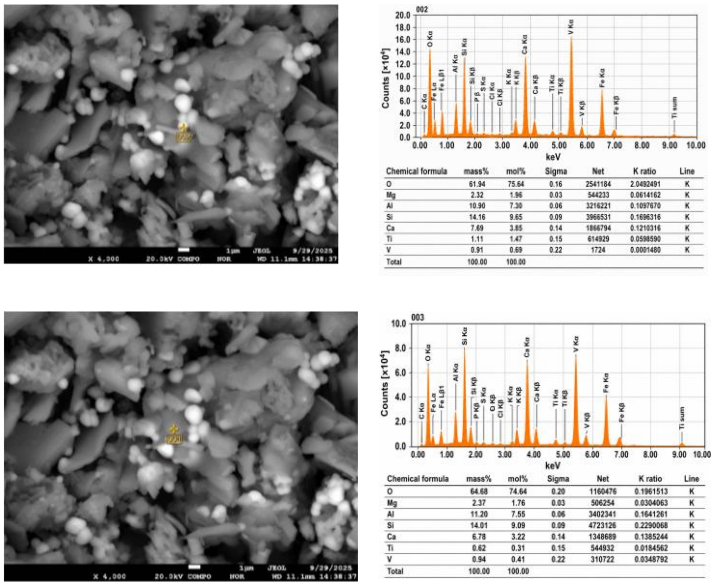

Chemical formula	mass%	mol%	Sigma	Net	K ratio	Line
O	61.94	75.64	0.16	2541184	2.0492491	K
Mg	2.32	1.96	0.03	544233	0.0614162	K
Al	10.90	7.30	0.06	3216221	0.1097670	K
Si	14.16	9.65	0.09	3966531	0.1696316	K
Ca	7.69	3.85	0.14	1866794	0.1210316	K
Ti	1.11	1.47	0.15	614929	0.0598590	K
V	0.91	0.69	0.22	1724	0.0001480	K
Total	100.00	100.00				

Chemical formula	mass%	mol%	Sigma	Net	K ratio	Line
O	64.68	74.64	0.20	1160476	0.1961513	K
Mg	2.37	1.76	0.03	506254	0.0304063	K
Al	11.20	7.55	0.06	3402341	0.1641261	K
Si	14.01	9.09	0.09	4723126	0.2290068	K
Ca	6.78	3.22	0.14	1348689	0.1385244	K
Ti	0.62	0.31	0.15	544932	0.0184562	K
V	0.94	0.41	0.22	310722	0.0348792	K
Total	100.00	100.00				

Fig. 12 Higher-magnification EPMA image and point-analysis spectra of the non-magnetic fraction (×4000).

As shown in **Figs. 11** and **12**, the non-magnetic fraction exhibits a markedly different microstructure from the Fe-rich magnetic product. The particles are predominantly angular, plate-like, and aggregated, and no coarse metallic Fe domains comparable to those observed in **Fig. 10** are evident. Point analyses indicate a chemically heterogeneous oxide–silicate matrix containing Si, Ca, Mg, Al, and Ti, while selected Ti-rich regions contain only low or locally undetectable Fe concentrations. This local Fe depletion is consistent with effective microscale partitioning of iron away from Ti-bearing domains during roasting. The observation should, however, be interpreted as local microanalytical evidence rather than as proof of complete Fe removal, because bulk chemical analysis confirms that residual iron remains in the non-magnetic product.

Taken together, the chemical, XRD, and EPMA results provide mutually consistent evidence of pronounced Fe–Ti phase redistribution during reduction roasting. Reduction promotes the formation and coalescence of metallic Fe-rich particles, whereas titanium becomes concentrated predominantly in non-magnetic oxide phases, including rutile and magnesium titanate. This redistribution generates the magnetic contrast required for efficient downstream separation. The results therefore support a process interpretation involving coupled iron reduction, phase transformation, and microstructural segregation rather than reduction alone. A complete mechanistic description of the transient chloride- and fluoride-assisted reactions would, however, require direct characterization of intermediate and gaseous species.

4. Conclusions

Low-temperature chloride-assisted reduction roasting followed by magnetic separation enabled effective Fe–Ti partitioning from high-titanium titanomagnetite while simultaneously providing a pathway for the valorization of chloride-rich titanium production waste. Response-surface analysis identified roasting temperature as the dominant process variable and revealed pronounced nonlinear effects of reagent dosage, defining a broad high-performance operating region rather than a single sharply constrained optimum. Multi-response optimization, supported by experimental validation and consideration of reagent consumption, established 1200 °C, 20 wt.% semi-coke, 30 wt.% SMTC, and 4 wt.% CaF_2 as the practically optimal operating conditions. Under these conditions, the magnetic fraction contained 91.24 wt.% Fe at an iron recovery of 91.94%, whereas the non-magnetic fraction contained 62.78 wt.% TiO_2 at a TiO_2 recovery of 96.04%. The selected operating point therefore represents a balanced Fe–Ti separation response rather than the maximization of any single metallurgical index. Comparative experiments further demonstrated that SMTC outperformed conventional NaCl in promoting iron metallization and titanium partitioning into the non-magnetic fraction. This enhanced performance is consistent with the beneficial influence of the multicomponent chloride matrix of SMTC on reduction and phase redistribution; however, the individual contributions of specific chloride species remain to be resolved by further mechanistic investigation. XRD identified Ti-bearing α-Fe as the largest individual crystalline phase in the magnetic product, accompanied by residual magnetite and smaller amounts of hematite and ilmenite, whereas the non-magnetic product was enriched in rutile, magnesium titanate, and silicate phases. EPMA further revealed coarse spheroidized Fe-rich particles and preferential concentration of Ti-bearing oxide phases in the non-magnetic product, providing complementary microstructural evidence of Fe–Ti redistribution during roasting and subsequent magnetic separation. Collectively, the statistical, metallurgical, mineralogical, and microstructural evidence indicates that effective Fe–Ti separation results from the coupled effects of iron reduction, phase transformation, and microstructural segregation rather than from reduction alone. The combined use of semi-coke, SMTC, and CaF_2 therefore provides a technically promising route for selective Fe–Ti separation from high-titanium titanomagnetite, while converting chloride-rich titanium production waste from an industrial residue into a functional metallurgical process additive.

Acknowledgements: This research is funded by the Committee of Industry of the Ministry of Industry and Construction of the Republic of Kazakhstan under program-targeted funding for scientific research for 2024–2026, BR23991563: «Creation of Innovative Resource-Saving Technologies for Mining and Integrated Processing of Mineral and Technogenic Raw Materials».

REFERENCES

1. Vorobkalo, N., Baisanov, A., Makhambetov, Y., Mynzhasar, Y., & Nurgali, N. (2023). Technological research of process for producing titanium rich slag and complex titanium-containing ferroalloy. Heliyon, 9(8). https://doi.org/10.1016/j.heliyon.2023.e18989
2. Kholmirzaev, N., Turakhodjaev, N., Saidmakhamadov, N., Khasanov, J., Bektemirov, A., & Sadikova, N. (2024, May). Effects of titanium (Ti) contents on the wear resistance of low-alloy steel alloys. In *E3S Web of Conferences* (Vol. 525, p. 03003). EDP Sciences. https://doi.org/10.1051/e3sconf/202452503003
3. Maldybayev, G., Korabayev, A., Sharipov, R., Al Azzam, K. M., Negim, E. S., Baigenzhenov, O., ... & Shayakhmetova, R. (2024). Processing of titanium-containing ores for the production of titanium products: A comprehensive review. *Heliyon*, *10*(3). https://doi.org/10.1016/j.heliyon.2024.e24966

4. Maruthuvakudi Venkatram, N., Alsabeeha, S., R Weston, N., Liu, Z., & Mavris, D. N. (2024). Life cycle assessment and risk management of titanium for aerospace applications. In *AIAA SCITECH 2024 Forum* (p. 1216). https://doi.org/10.2514/6.2024-1216
5. Maldybayev, G. K., Korabayev, A. S., Shayakhmetova, R. A., Khabiyev, A. T., Baigenzhenov, O. S., Sharipov, R. H., & Amirkhan, A. A. (2024). Separation of iron and titanium from titanium magnetite raw materials by low-temperature treatment and magnetic separation. *Case Studies in Chemical and Environmental Engineering*, *10*, 100848. https://doi.org/10.1016/j.cscee.2024.100848
6. Tahooni Bonab, S., Abdollahi, H., & Abbaspour, A. (2025). The hydrometallurgical approach in the production of a high content of titanium dioxide (TiO2) from ilmenite, direct hydrochloric and sulfuric acid leaching and pre-treatment methods: A review. *Mineral Processing and Extractive Metallurgy Review*, *46*(4), 537-553. https://doi.org/10.1080/08827508.2024.2346654
7. Goncharov, K. V., Agamirova, A. S., Olyunina, T. V., & Sadykhov, G. B. (2025). Processing of Titanomagnetite Concentrate to Produce Slags Suitable for Further Recovery of Titanium and Vanadium. *Russian Metallurgy (Metally)*, *2025*(1), 225-229. https://doi.org/10.1134/S0036029525701058
8. Oke, E. A., Potgieter, J. H., Nkhoesa, D., & Dyk, L. D. V. (2025). Vanadium, titanium, and iron extraction from titanomagnetite ore by salt roasting and 21st-century solvents. *Separations*, *12*(10), 285. https://doi.org/10.3390/separations12100285
9. Yan, Zh., Zhang, Y., Zheng, S. L., Zhang, Y., Sun, P., Song, Z., Safdar, F., & Qi, T. (2022). Preparation of titanium mineral from vanadium titanomagnetite concentrates by hydrogen reduction and acid leaching. *Transactions of Nonferrous Metals Society of China*, *32*(9), 3099-3109. https://doi.org/10.1016/S1003-6326(22)66006-0
10. Myrzakulov, M. K., Jumankulova, S. K., Barmenshinova, M. B., Martyushev, N. V., Skeeba, V. Y., Kondratiev, V. V., & Karlina, A. I. (2024). Thermodynamic and Technological Studies of the Electric Smelting of Satpaevsk Ilmenite Concentrates. *Metals*, *14*(11), 1211. https://doi.org/10.3390/met14111211
11. Qu, Y., Xing, L., Gao, M., Zhao, S., Ren, Q., Li, L., & Long, Y. (2024). Progress and Prospects for Titanium Extraction from Titanium-Bearing Blast Furnace Slag. *Materials*, *17*(24), 6291. https://doi.org/10.3390/ma17246291
12. Akhmetova, K., Gladyshev, S., Abdulvaliev, R., Imangaliyeva, L., Manapova, A., & Kasymzhanova, A. (2025). Efficiency of Soda-Technology Carbothermal Smelting of Thermoactivated Ilmenite Concentrate with Aluminosilicate Mineralization. *Minerals*, *15*(9), 906. https://doi.org/10.3390/min15090906
13. Trinh, H. B., Kim, S., Lee, J., & Oh, S. (2023). Efficient Recovery of Vanadium and Titanium from Domestic Titanomagnetite Concentrate Using Molten Salt Roasting and Water Leaching. *Materials*, *16*(21), 6918. https://doi.org/10.3390/ma16216918
14. Yan, Z., Zheng, S., Zhang, Y. *et al.* (2025). Titanium in the Industrial Titanomagnetite Metallurgy Processes: Effects and Recovery. *JOM,* 77, 3354. https://doi.org/10.1007/s11837-025-07214-4
15. Zhang, W., Zhu, Z., & Cheng, C. Y. (2011). A literature review of titanium metallurgical processes. *Hydrometallurgy*, *108*(3-4), 177-188. https://doi.org/10.1016/j.hydromet.2011.04.005
16. Guo, K., Wang, S., Song, R., & Zhang, Z. (2021). Leaching titaniferous magnetite concentrate by alkaline aqueous solution. *Mining, Metallurgy & Exploration*, *38*(4), 1721-1730. https://doi.org/10.1007/s42461-021-00387-x
17. Pelevin, A. E. (2025). Application of dry magnetic separation in beneficiation processes for ilmenite-titanomagnetite ores. *Obogashchenie Rud*, *2*, 32-37. https://doi.org/10.17580/or.2025.02.05
18. Connelly, D. (2024). The changing technology trends in processing titaniferous magnetite. *Canadian Metallurgical Quarterly*, *63*(3), 657-670. https://doi.org/10.1080/00084433.2024.2358260
19. Karshyga, Z., Ultarakova, A., Lokhova, N., Yessengaziyev, A., & Kassymzhanov, K. (2022). Processing of titanium-magnesium production waste. *Journal of Ecological Engineering*, *23*(7). https://doi.org/10.12911/22998993/150004
20. Ultarakova, A., Karshyga, Z., Lokhova, N., Yessengaziyev, A., Kassymzhanov, K., & Mukangaliyeva, A. (2022). Studies on the Processing of Fine Dusts from the Electric Smelting of Ilmenite Concentrates to Obtain Titanium Dioxide. *Materials*, *15*(23), 8314. https://doi.org/10.3390/ma15238314
21. Orynbayev, B., Toishybek, A., Ultarakova, A., Baigenzhenov, O., & Mukangaliyeva, A. (2025). Study of scandium sorption from a solution of leached waste from titanium production with hydrochloric acid. *Acta Metallurgica Slovaca*, *31*(3), 194-199. https://doi.org/10.36547/ams.31.3.2232
22. Nizamoğlu, H., Turan, M. D., Sarı, Z. A., & Babayeva, P. (2024). Sustainable green industry work: recovery of copper slag with mill scale leaching reactant optimized by response surface methodology (RSM). *Journal of Sustainable Metallurgy*, *10*(4), 2501-2520. https://doi.org/10.1007/s40831-024-00944-w
23. Yulusov, S., Khabiyev, A., Merkibayev, Y., Sarsembayeva, M., Bakhytuly, N., Konyratbekova, S., & Adam, M. R. (2026). Application of the surface response methodology (RSM) to optimise alkaline leaching of vanadium and molybdenum from man-made raw materials. *Acta Metallurgica Slovaca*, *32*(1), 21-28. https://doi.org/10.36547/ams.32.1.2259
24. Liu, S. S., Guo, Y. F., Qiu, G. Z., & Jiang, T. (2020). Mechanism of vanadic titanomagnetite solid-state reduction. *Rare Metals*, *39*(11), 1348-1352. https://doi.org/10.1007/s12598-014-0294-3
25. Xu, L., Liu, H., Cheng, D., Zhong, Q., Peng, Z., Li, G., & Jiang, T. (2022). Efficient double-layer sintering of titanomagnetite concentrate. *Scientific Reports*, *12*(1), 6355. https://doi.org/10.1038/s41598-022-10405-7
26. Geng, C., Sun, T. C., Ma, Y. W., Xu, C. Y., & Yang, H. F. (2017). Effects of embedding direct reduction followed by magnetic separation on recovering titanium and iron of beach titanomagnetite concentrate. *Journal of Iron and Steel Research International*, *24*(2), 156-164. https://doi.org/10.1016/S1006-706X(17)30022-5
27. Zhao, Y., Sun, T., & Wang, Z. (2021). Extraction of iron from refractory titanomagnetite by reduction roasting and magnetic separation. *ISIJ International*, *61*(1), 93-99. https://doi.org/10.2355/isijinternational.ISIJINT-2020-251
28. Gao, E. X., Sun, T. C., Yu, C. X., & Liu, Z. G. (2016). Effects of Coal Types on the Separation of Iron and Titanium in Titanomagnetite by Direct Reduction-Magnetic Separation. *Journal of Northeastern University (Natural Science)*, *37*(5), 716. https://doi.org/10.12068/j.issn.1005-3026.2016.05.023
29. Chen, D., Zhao, L., Liu, Y., Qi, T., Wang, J., & Wang, L. (2013). A novel process for recovery of iron, titanium, and vanadium from titanomagnetite concentrates: NaOH molten salt roasting and water leaching processes. *Journal of hazardous materials*, *244*, 588-595. https://doi.org/10.1016/j.jhazmat.2012.10.052
30. Wu, S., Li, Z., Sun, T., Lu, S., & Cao, Z. (2022). Individual enrichment of titanium and iron from low-titanium beach titanomagnetite via preconcentration-reduction roasting and magnetic separation with calcium fluoride. *Powder Technology*, *409*, 117810. https://doi.org/10.1016/j.powtec.2022.117810
31. Wang, Zh., Chen, S., Chen, L., Liang, B., Luo, D. (2025). Enhancing iron and titanium recovery efficiency via coal-based direct reduction of vanadium-titanium magnetite raw ore. *Transactions of Nonferrous Metals Society of China*, *35*(10), 3480-3492. https://doi.org/10.1016/S1003-6326(25)66894-4